

# Stretchable Conductive Composites from Cu–Ag Nanowire Felt

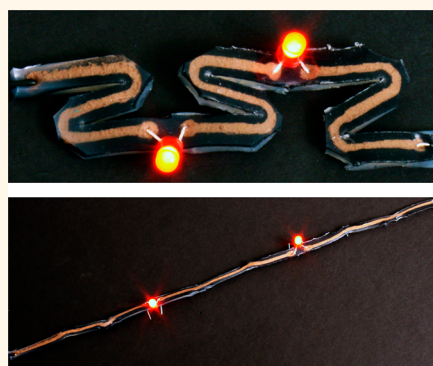
Matthew J. Catenacci,<sup>1b</sup> Christopher Reyes,<sup>1b</sup> Mutya A. Cruz, and Benjamin J. Wiley\*

Department of Chemistry, Duke University, Durham, North Carolina 27708, United States

## S Supporting Information

**ABSTRACT:** Materials that retain a high conductivity under strain are essential for wearable electronics. This article describes a conductive, stretchable composite consisting of a Cu–Ag core–shell nanowire felt infiltrated with a silicone elastomer. This composite exhibits a retention of conductivity under strain that is superior to any composite with a conductivity greater than  $1000 \text{ S cm}^{-1}$ . This work also shows how the mechanical properties, conductivity, and deformation mechanism of the composite changes as a function of the stiffness of the silicone matrix. The retention of conductivity under strain was found to decrease as the Young's modulus of the matrix increased. This was attributed to void formation as a result of debonding between the nanowire felt and the elastomer. The nanowire composite was also patterned to create serpentine circuits with a stretchability of 300%.

**KEYWORDS:** stretchable conductors, copper nanowires, nanowire composite, Young's modulus, stretchable circuits



Materials that are both conductive and stretchable are essential for the construction of stretchable circuits for use in wearables, robotics, bioelectronics, and energy storage.<sup>1–6</sup> While stretchable materials with low-conductivity ( $<1 \text{ S cm}^{-1}$ ) can be used for strain sensors or touch sensors, stretchable wiring and interconnects require conductivities as close as possible to copper ( $5.8 \times 10^5 \text{ S cm}^{-1}$ ). In addition, such materials should retain their conductivity under high strain ( $>50\%$ ) after many cycles of stretching.

Figure 1 shows a concise summary of the properties of some stretchable, conductive bulk composites. These include elastomers containing single-walled carbon nanotubes (SWNTs),<sup>1,7,8</sup> poly(3,4-ethylenedioxythiophene) (PEDOT),<sup>9</sup> polyaniline (PANI),<sup>10</sup> Ag microflakes (Ag MFs),<sup>11–13</sup> Ag nanowires (Ag NWs), and Cu nanowires (Cu NWs).<sup>14–17</sup> While high conductivities have also been achieved in stretchable thin films, they have been left out of Figure 1 because their modes of mechanical deformation differ substantially from those of the bulk composites discussed in this work.<sup>18,19</sup> Among the previously made stretchable composites, those containing Ag MFs clearly stand out as exhibiting a combination of high initial conductivity, as well as retention of conductivity after 50 cycles of stretching to 50% strain. However, in order to retain conductivity after multiple cycles of stretching, it was necessary for the Ag MFs in these composites to be sintered together to form a continuous network. For example, although there are three Ag MF results in Figure 1A, only the sample in which the Ag was sintered together with photonic curing<sup>13</sup> exhibited a minimal (80%) increase in resistance after multiple cycles of stretching, and thus appears in Figure 1B. The other samples

that were not sintered exhibited an increase in resistance greater than 2 orders of magnitude after 50 cycles of stretching to 50% strain. This difference may be due to the Ag MFs being pulled apart within the composite when they are not sintered together. In contrast, a sintered, porous network of Ag MFs may deform upon stretching with relatively minimal breakup of the interconnected particle network. Although these Ag MF results are highly informative and can provide direction for future work, Ag is rare, expensive, and has a large carbon footprint. A future in which millions of people wear clothing imbued with stretchable circuitry cannot be built upon such a rare and costly element.

Cu is 1000 times more abundant, 100 times less expensive, and has a carbon footprint 25 times lower than Ag.<sup>20</sup> Previous work with Cu NW-based stretchable composites demonstrated the potential of Cu NWs to achieve high conductivities at low volume fractions due to their high aspect ratios ( $>2.2 \times 10^3$ ). For example, Cu NWs mixed with poly(styrene-*block*-butadiene-*block*-styrene) (SBS) rubber obtained a conductivity of  $844 \text{ S cm}^{-1}$  at a loading of 7 vol %.<sup>17</sup> However, it is not practical to use bare copper nanowires because of their tendency to oxidize. In addition, this previous Cu NW composite exhibited poor retention of conductivity under strain, likely because the nanowires were mixed into an ink and were not annealed into an interconnected network.

Received: February 2, 2018

Accepted: March 14, 2018

Published: March 14, 2018

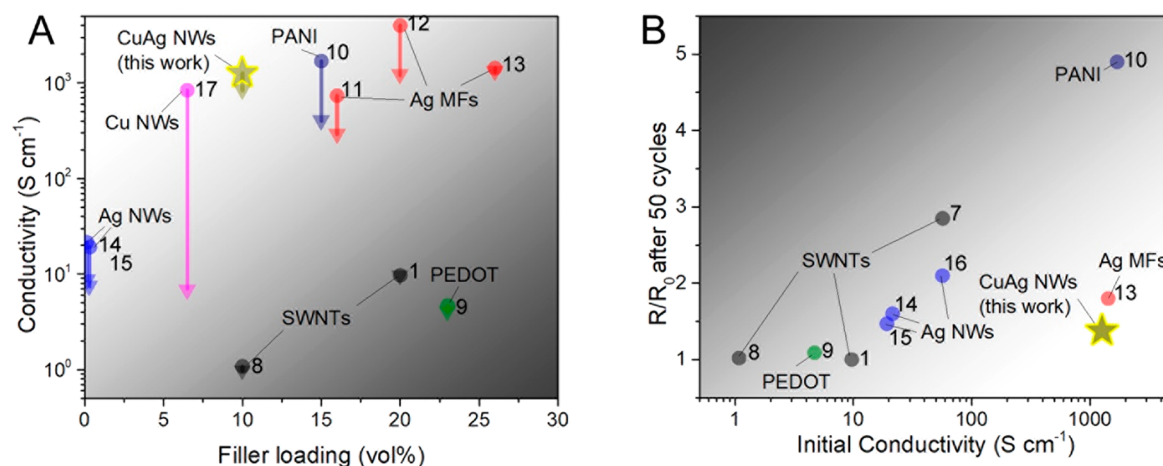


**Figure 1.** (A) Conductivity of stretchable, conductive bulk composites at 0% (circle) and 100% (triangle) strain as a function of conductive filler loading. (B)  $R/R_0$  after 50 cycles of stretching to 50% strain. Numbers indicate references.

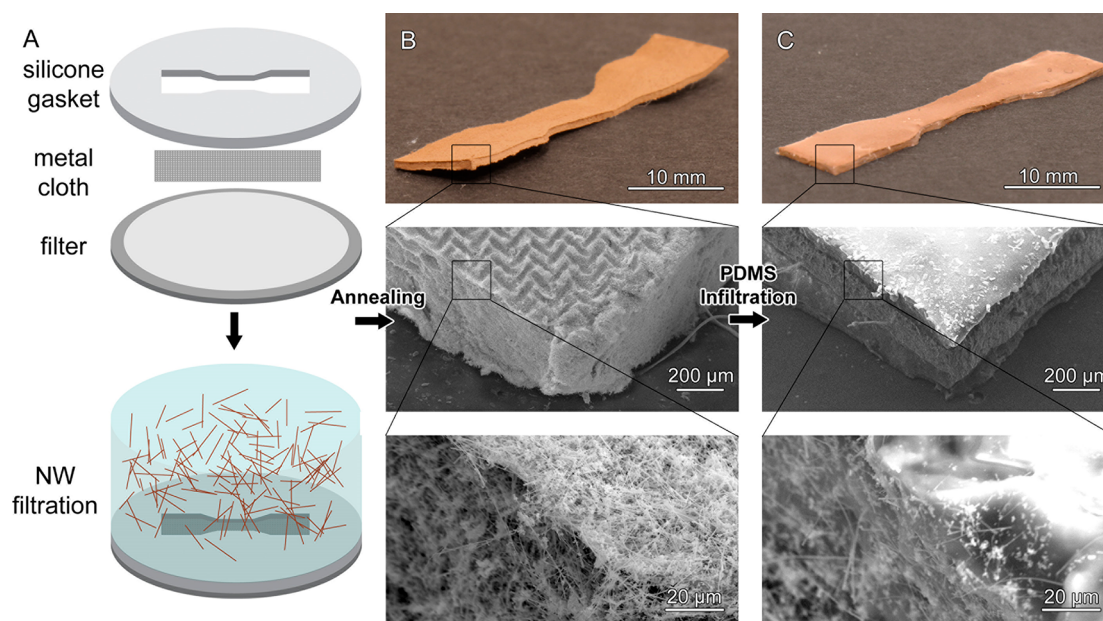


**Figure 2.** (A) Cu–Ag NWs were filtered through a silicone gasket onto a metal cloth to create a NW felt in the shape of the hole in the gasket. (B) Photograph and SEM image of felt after annealing and (C) after PDMS infiltration.

We hypothesized that these problems of material sustainability and performance for stretchable conductors could be addressed by creating stretchable composites from Cu–Ag core–shell nanowire (Cu–Ag NW) felts. Cu–Ag NWs can be synthesized at relatively low cost (currently  $\sim$ \\$7 per gram),<sup>21</sup> can form highly conductive composites, and are highly resistant to oxidation.<sup>22</sup> To ensure that the Cu–Ag NW composites retained their conductivity under strain, we developed a simple fabrication approach in which nanowires were filtered from solution and annealed together to form a highly conductive, freestanding felt. This approach ensured that the Cu–Ag NWs were electrically connected before infiltration with PDMS, and enabled the creation of stretchable composites with a conductivity of  $1270\text{ S cm}^{-1}$ , a value comparable to previous composites made with Ag MFs. In addition, the Cu–Ag NW composites exhibited only a 37% increase in resistance after 50 cycles of stretching to 50% strain, which is the lowest increase among any material with a conductivity  $>1000\text{ S cm}^{-1}$ . We show that the conductivity loss under strain is highly dependent

on the stiffness of the elastic matrix, a difference that appears to be due to the formation of voids upon stretching. Finally, we illustrate that the stretchable nanowire composite can be fabricated into serpentine patterns that retain their conductivity to strains of 300%. The combination of high performance and improved sustainability make Cu–Ag NW composites a promising material upon which to build a stretchable electronics industry.

## RESULTS AND DISCUSSION

**Fabrication and Conductivity.** The procedure for composite manufacturing is illustrated in Figure 2A. Cu–Ag nanowires were first synthesized as described previously and in the experimental section.<sup>21,22</sup> The nanowires were filtered through a rubber gasket onto a metal cloth to form dogbone-shaped test specimens according to ASTM D412 for tensile testing. The length, width and thickness of the test specimens were 10 mm, 3 mm, and  $250\text{ }\mu\text{m}$ , respectively (see Figure S1 for full schematic). The average density of the nanowire felt

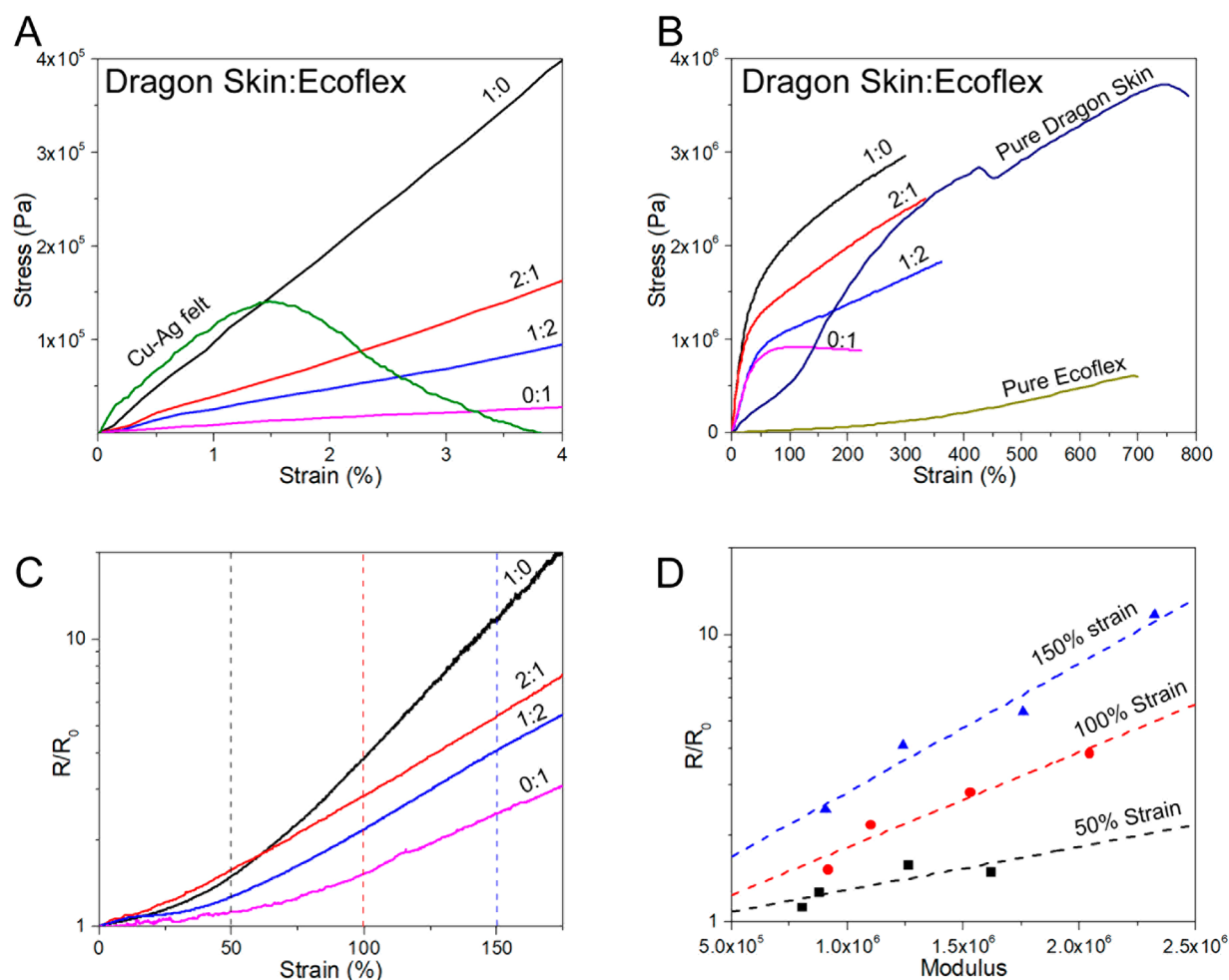


**Figure 3.** (A) Stress vs strain performance for the Cu–Ag NW felt, as well as various Cu–Ag NW PDMS composites containing different ratios of Dragon Skin to Ecoflex. (B) Stress vs strain curves for Cu–Ag NW composites. (C)  $R/R_0$  vs strain for the Cu–Ag NW composites. (D)  $R/R_0$  vs modulus at 50, 100, and 150% strain. Strain rates were  $1\% \text{ s}^{-1}$ .

prior to infiltration (Figure 2B) over three replicates was  $0.87 \pm 0.04 \text{ mg/mL}$ . This density corresponds to a porosity of  $90.5 \pm 0.4\%$  based on a weighted average of the densities of Cu (85%) and Ag (15%). After filtration, the NWs were annealed at a variety of temperatures for 30 min to determine which temperature yielded the highest conductivity prior to infiltration (Figure S2). An annealing temperature of  $150 \text{ }^\circ\text{C}$  resulted in the highest conductivity ( $2040 \pm 35 \text{ S cm}^{-1}$ ). This conductivity is 1.6 times higher than the air-dried sample before annealing ( $1270 \pm 610 \text{ S cm}^{-1}$ ). The conductivity of the annealed NW felts is only 28 times less conductive than Cu with a porosity of 90% ( $5.8 \times 10^4 \text{ S cm}^{-1}$ ).

After infiltration with PDMS (Figure 2C), a 40% decrease in electrical conductivity was observed ( $1220 \pm 630 \text{ S cm}^{-1}$ ), likely because the insulating elastomer increased the contact resistance between the four-point probe and the conductive filler. However, this conductivity is still only 47 times less conductive than bulk Cu at a similar porosity, and is comparable to previous results with Ag MFs at filler loadings double that of the Cu–Ag NW composite (see Figure 1A). The infiltrated Cu–Ag NW network is also four times more conductive than identical Cu–Ag NWs blended into polycaprolactone at a similar concentration (12 vol %).<sup>21</sup>

**Effect of Matrix Stiffness on Conductivity as a Function of Strain.** In order to examine the effect of the

stiffness of the elastomer matrix on the ability of the composite to retain its conductivity under strain, the Cu–Ag NW felt was infiltrated with relatively low-stiffness and high-stiffness PDMS elastomers at four different ratios. The low-stiffness PDMS is Ecoflex 00–30 (0.07 MPa at 100% strain), and the high-stiffness PDMS is Dragon Skin 30 (0.59 MPa at 100% strain). We will hereafter refer to these materials as Ecoflex and Dragon Skin. Figure 3A shows that, before infiltration, the annealed Cu–Ag NW network is very brittle. Fracture initiates at 1.5% strain and is complete at approximately 4% strain. After infiltration with PDMS, the composite does not fracture until strains of 250–350% (Figure 3B). Figure 3B also shows that the presence of the NW network within PDMS greatly increases its stiffness. Compared to the pure version of the elastomer, the stiffness of the Dragon Skin and Ecoflex composites increased by a factor of 3.4 and 13, respectively. These mechanical tests illustrate the Cu–Ag NW felt infiltrated with PDMS exhibits a stiffness closer to that of the nanowire felt than that of the elastomer, even though the nanowires comprise only 10% of the volume of the composite. Thus, it seems that the deformation of the nanowire network within the elastomer may be dominating the stress–strain behavior of these materials. In addition, it is clear that the presence of the elastomer matrix prevents fracture and breakup of the nanowire felt, facilitating its deformation under an applied stress.

Figure 3A,B shows that, as expected, the stiffness of the composite increases with the amount of Dragon Skin present in the infiltrated PDMS relative to the amount of Ecoflex. Figure 3C shows that this increase in stiffness had a significant effect on the ability of the composites to retain their initial conductivity under an initial applied strain. The Ecoflex composite exhibits an increase in resistance, denoted by  $R/R_0$ , of only 1.12, 1.52, and 2.46 at strains of 50%, 100%, and 150% respectively. In comparison, the  $R/R_0$  of the Dragon Skin-NW composites is higher, at 1.49, 3.86, and 11.7 at the same strains. With the intermediate blends of Ecoflex and Dragon Skin, intermediate values of  $R/R_0$  were observed. Figure 3D summarizes the effect of matrix stiffness on retention of conductivity by plotting the  $R/R_0$  vs modulus at strains of 50%, 100%, and 150%. The four modulus values are from Ecoflex, Dragon Skin, as well as the 2:1 and 1:2 blends of Dragon Skin:Ecoflex. This panel illustrates there is a clear trade-off between the stiffness of the matrix and the conductivity that can be retained as the composite is stretched.

Although there have been many previous studies of the electrical conductivity of PDMS composites, and it has been observed how changing the type or concentration of conductive filler can influence stiffness and electrical properties,<sup>23–29</sup> we can find no previous studies on the effect of the stiffness of the elastomer matrix on the ability of the composite to retain its electrical properties under strain. In order to gain further insights into the mechanism of this phenomena, we examined whether there was any difference in the mechanism of deformation for Dragon Skin and Ecoflex composites. Figure 4 displays photographs of the Cu–Ag felt, the Dragon Skin

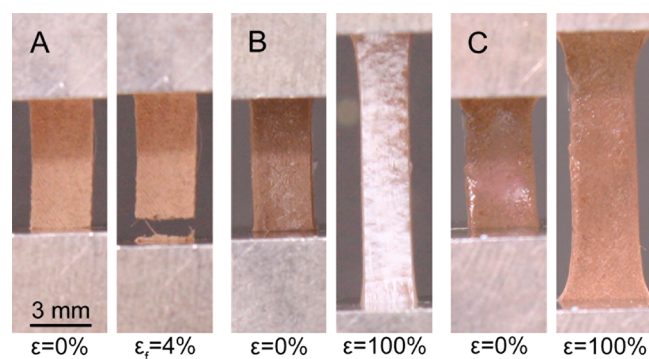


**Figure 4.** Images showing the difference in the stretchability and void formation for the (A) Cu–Ag NW felt (B) Dragon Skin-NW composite and (C) Ecoflex-NW composite during the initial strain.

composite, and the Ecoflex composite at 0 and 100% strain. As seen in Figure 4A, the Cu–Ag NW felt without PDMS is brittle and fractures at low strain. The Dragon Skin composite (Figure 4B) turns from orange to white under strain, but no obvious color change was observed for the Ecoflex composite (Figure 4C). This suggested the Dragon Skin composite formed voids under strain, while the Ecoflex composite did not. This difference in deformation response was confirmed with SEM imaging. Figure 5A,D show both the Ecoflex and Dragon Skin composites appeared to be free of voids initially. Although nanowires appeared to align in both composites at 100% strain (Figure 5B,E), only the Dragon Skin contained a large amount of voids in the strained state. When the Ecoflex was brought back to a strain of 0%, there were no noticeable voids present within the composite. In contrast, the voids were retained in the

Dragon Skin composite and became buckled as it was relaxed to a strain of 0% (Figure 5F).

These observations suggest that the reason for the greater decrease in conductivity as a function of strain for composites containing stiffer PDMS is due to the formation of voids. Gent and Park previously studied the effect of elastomer stiffness on the formation of voids through cavitation and debonding in elastomers with rigid spherical inclusions.<sup>30</sup> They found that while the stress required for cavitation (expansion of microvoids) increases with increasing Young's modulus, the stress required for debonding decreases with increasing Young's modulus. This was attributed to the fact that lower-modulus materials are able to dissipate more energy during debonding through viscoelastic energy losses that occur during deformation of the sample.<sup>31</sup> Thus, the fact that Ecoflex is eight times less stiff than Dragon Skin may result in a stronger interfacial adhesion between the PDMS and the Cu–Ag NWs. This stronger adhesion may prevent void formation during debonding, and thus improve the retention of conductivity under strain for the Ecoflex composite.

**Cycling.** The Dragon Skin and Ecoflex composites were cycled 50 times to strains of 50% and 100% to examine how well the composites retained their conductivity over many cycles of stretching (Figure 6A,B). For the cycling to strains of 50%, both the Dragon Skin and Ecoflex composites exhibited an irreversible loss in conductance after the first complete cycle, with an  $R/R_0$  of 1.68 and 1.37, respectively. The resistance at 0 and 50% strain remained fairly stable over subsequent cycles, exhibiting a standard deviation of 0.04 and 0.02 for Dragon Skin and Ecoflex, respectively. We note that, after the first cycle, the resistance was lower in the strained state than for the relaxed state. The ratio between the  $R/R_0$  at 0 and 50% strain was  $1.12 \pm 0.09$  and  $1.15 \pm 0.05$  for the Dragon Skin and Ecoflex composites, respectively. Overall these composites demonstrated robust cycling durability and a modest change in resistance upon stretching to 50% strain.

At 100% strain, the Ecoflex composite still exhibits relatively stable resistance, but requires 3 cycles to achieve stable cycling. After 3 cycles, the maximum  $R/R_0$  is 2.65, and the ratio between the  $R/R_0$  for 0 and 50% strain is  $1.49 \pm 0.06$ . Significantly different behavior is observed for the Dragon Skin composite. The  $R/R_0$  increases for the first 5 cycles, then subsequently decreases until it becomes fairly stable after 40 cycles. The maximum  $R/R_0$  of the composite (5.94) occurred after the fifth cycle; the  $R/R_0$  max decreases to 3.64 at 0% strain after the 50th cycle.

Most previous studies of infiltrated nanowire networks did not observe a higher conductivity in the strained state after cycling, but we are using much higher concentrations of conductive material ( $\sim 10$  vol %) than was used in those previous studies ( $< 1$  vol %). Studies that have observed such phenomena include those that examined the properties of 2 vol % steel wool infiltrated with PDMS,<sup>32</sup> 32 vol % PEDOT:PSS in polyurethane,<sup>33</sup> 48 vol % Ag MFs in bubbled polyurethane,<sup>34</sup> and 63 vol % carbon black in natural rubber.<sup>35</sup> In an attempt to provide additional insights into why the conductivity is higher in the strained state, we examined how the stress–strain and  $R/R_0$ -strain behavior changed during cycling. Figure 7A,B shows that there is a large hysteresis and plastic deformation in the first cycle of stretching for both composites; Ecoflex and Dragon Skin exhibit irreversible strains of 54% and 34%, respectively. In comparison, Figure S3A,B shows the pure Dragon Skin and Ecoflex exhibit little hysteresis, as well as

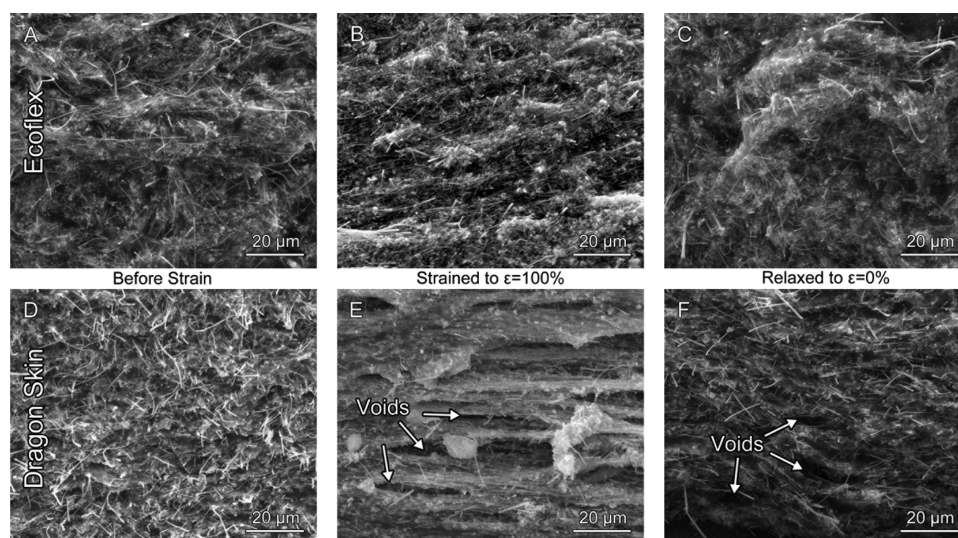


Figure 5. (A,D) SEM images of the Ecoflex and Dragon Skin composites before strain, (B,E) at 100% strain, and (C,F) after relaxation back to 0% strain. Voids are present in the Dragon Skin composite, but not in the Ecoflex composite.

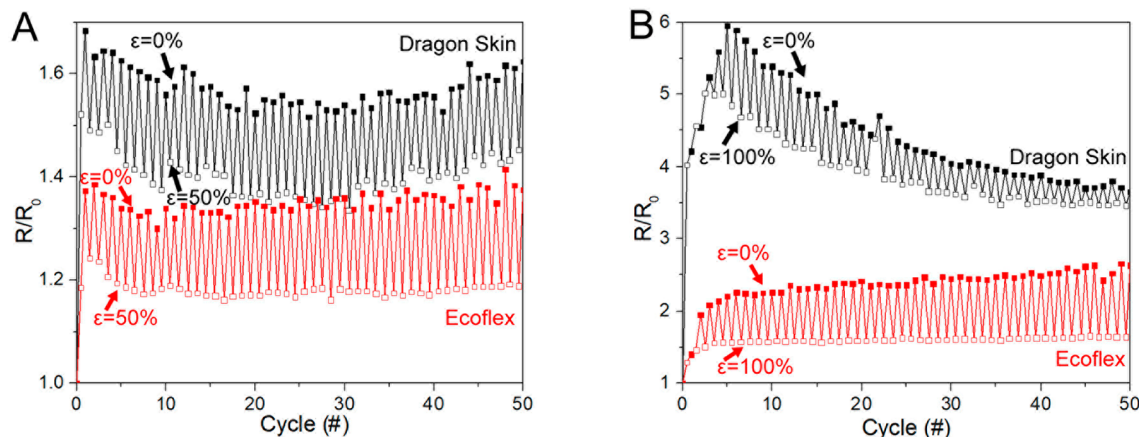


Figure 6. (A)  $R/R_0$  behavior over 50 cycles at 50% strain and (B) 100% strain. Strain rates were  $20\% \text{ s}^{-1}$ .

plastic deformations of 4 and 2%, respectively. There is no additional plastic deformation in subsequent cycles, but the composite continued to soften. Such softening is often observed for filler rubbers and is termed the Mullins' effect.<sup>36</sup> There is no consensus as to the mechanism behind the Mullins' effect, and it can vary between composites, but it is often ascribed to sliding of filler material within the composite,<sup>37</sup> and/or debonding between the filler material and the matrix, leading to the generation of voids.<sup>38</sup> The former is difficult to discern, but the latter is obviously occurring in the case of the Dragon Skin composite, as is shown in Figures 5C and 5F.

Figures 7C and 7D show the  $R/R_0$  continuously increases until the maximum strain of 100% during the first cycle. This is consistent with the fact that the  $R/R_0$  increased during the first cycles in Figure 6. By cycle 51, the  $R/R_0$  increases to a maximum of 5.83 at 50% strain for the Ecoflex composite, and a maximum of 5.57 at 38% strain for the Dragon Skin composite. Additional strain to 100% decreased the  $R/R_0$  to 1.92 and 2.25 for the Ecoflex and Dragon Skin, respectively. The strain at which the maximum values of  $R/R_0$  for each composite occurred are nearly identical to the extent of plastic deformation that occurred during the first cycle (54% for Ecoflex, 34% for Dragon Skin). We hypothesize that as the

material is strained from the relaxed state up until the point at which plastic deformation occurred, the buckled voids unbuckle in the Dragon Skin, reducing the overall number of electrical contacts and reducing the conductivity of the material. After the point of plastic deformation and up to 100% strain, the voids undergo transverse compression and strands begin to align, increasing the number of electrical contacts and increasing the conductivity of the material. Such behavior was previously observed for a composite with voids containing 48 vol % Ag MFs in polyurethane.<sup>34</sup>

On the other hand, the Ecoflex composite does not contain voids but exhibits nearly identical  $R/R_0$  vs strain behavior. A study by Yamaguchi *et al.* observed similar conductivity vs strain behavior for a 63 vol % loaded carbon black in natural rubber, and suggested that the slippage, orientation, and alignment of carbon black aggregates under strain contributed to the enhanced conductivity under strain.<sup>35</sup> Given that the most relaxed state of the Ecoflex composite after the first cycle is the point at which plastic deformation occurred during the first cycle, strains below or above this strain will lead to compression or alignment of the nanowire networks, both of which could conceivably be responsible for the lower  $R/R_0$  at 0% and 100% strain. Therefore, although the mechanisms may differ, for both

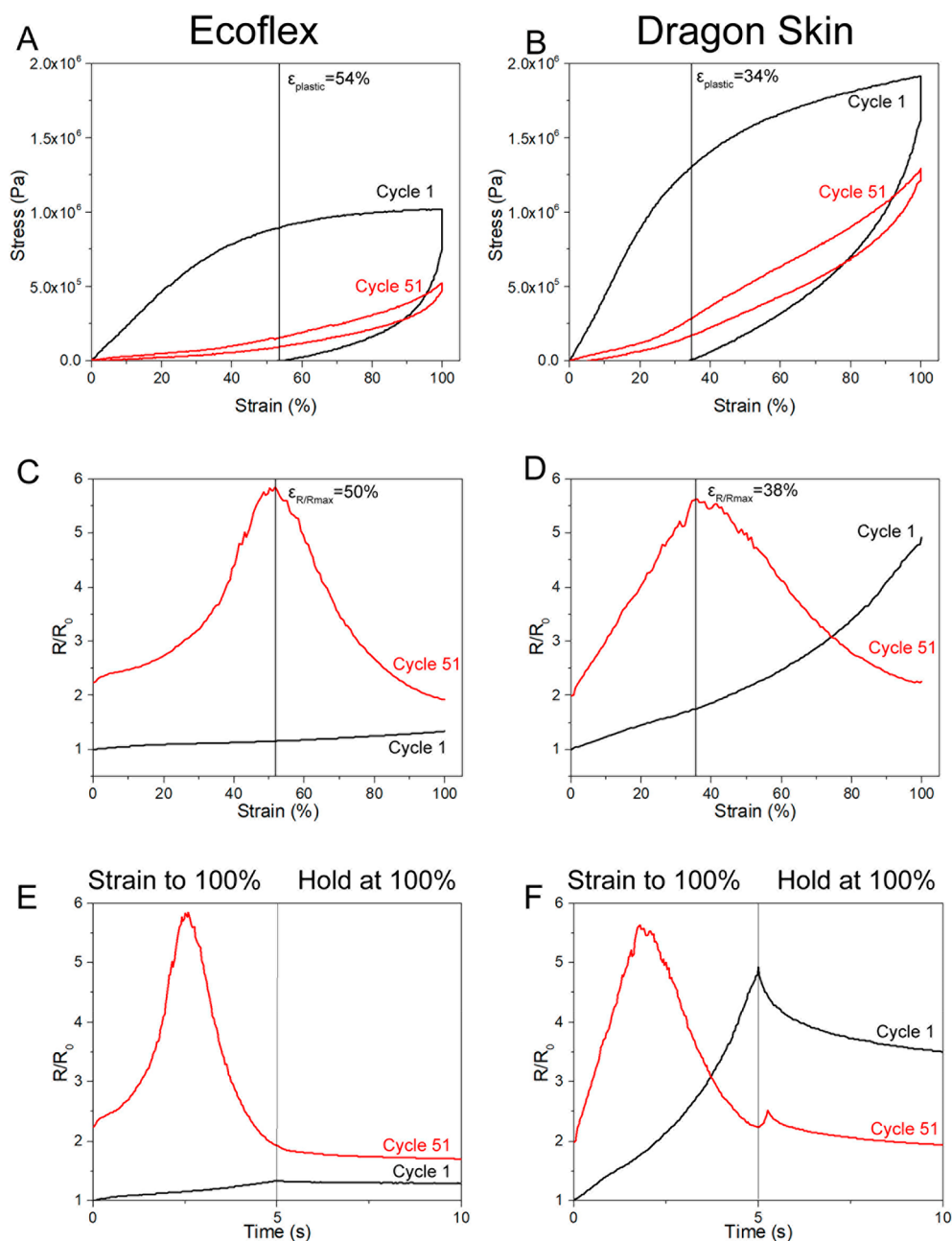


**Figure 7.** (A,B) Stress vs strain curves show the large plastic deformation and hysteresis during initial cycling for both Dragon Skin and Ecoflex composites. (C,D)  $R/R_0$  vs strain behavior for Dragon Skin and Ecoflex composites after the first and 51st cycle at 100% strain. (E,F) Time-dependent strain vs  $R/R_0$  behavior for Dragon Skin and Ecoflex composites after the first and 51st cycle at 100% strain. Strain rates were  $20\% \text{ s}^{-1}$ .

composites it appears that the alignment of NWs that occurred during the first strain cycle was permanent and made the composite more conductive in the strained state.

**Time-Dependent Behavior.** The other unusual observation is that the Dragon Skin composite regains some of the conductivity lost during the first 5 cycles of 100% strain, but the Ecoflex remains fairly stable. This effect may be attributed to the time-dependent behavior of the composites. It was previously observed that the resistance of multiwalled CNT-PDMS composites decreased over time when the composite was held at strain, and this behavior was attributed to stress relaxation.<sup>39</sup> We also observe a time-dependent decrease in the  $R/R_0$  for the strained Dragon Skin composite in this study (Figure 7F), but not for the Ecoflex (Figure 7E). The observed

drop in  $R/R_0$  after the first 5 cycles for Dragon Skin can be attributed to the decrease in the  $R/R_0$  that occurs over time for this stiffer composite. The difference in time-dependent  $R/R_0$  under strain for Ecoflex and Dragon Skin may be related to the different degree of debonding and void formation observed in these composites. As the Ecoflex composite is strained, the NWs align with the composite during the initial strain, and are held in place when strain is complete. This leads to a minimal decrease in  $R/R_0$  when the composite is held at strain. In contrast, as the Dragon Skin composite is strained, void formation results in a time dependent reordering of the NW network that results in a drop in  $R/R_0$ . Gaining additional insights into the mechanism of this process is experimentally challenging due to the difficulties in imaging the time-

dependent deformation of a three-dimensional network of nanowires, as well as calculating what the resistance of the nanowire network should be under various states of strain.

Although the effect of strain rate on the retention of conductivity is important for the practical use of a stretchable conductor, it is a dimension that is rarely explored. For example, the strain rates used in the previous studies listed in Figure 1 vary greatly from  $0.08\% \text{ s}^{-1}$  to  $5\% \text{ s}^{-1}$ , but none of those studies examined the effect of strain rate on the stress and  $R/R_0$  response.<sup>10,14</sup> Figure S4 shows the effect of strain rate on the stress and  $R/R_0$  for the Ecoflex and Dragon Skin composites. We selected a strain rate of  $1\% \text{ s}^{-1}$  to be in within the range of previous experiments in the literature, and a strain of  $20\% \text{ s}^{-1}$  to more accurately simulate the faster strain rates that would be seen in a wearable device.<sup>2,3,40,41</sup> The strain rate does not have much effect on the stress vs strain behavior for both the Ecoflex and Dragon Skin (Figure S4A,B). For the Ecoflex composite, the  $R/R_0$  vs strain is identical at the two strain rates (Figure S4C,D). However, for the Dragon Skin composite the slope of the  $R/R_0$  vs strain curve is larger for the  $20\% \text{ s}^{-1}$  strain rate during the first 20% of strain, after which the slopes were similar. This increase in  $R/R_0$  may be associated with the time-dependent effects discussed with respect to Figures 7E,F, as less time is available for the NW network to align and reduce its  $R/R_0$  under high rates of strain. Thus, we see that the matrix stiffness can not only affect the static increase in  $R/R_0$ , but also its time-dependent behavior.

**Patterning.** In addition to the ability to make highly conductive composites that retain their conductivity under strain, the filtration-based fabrication approach reported here can be used to pattern the Cu–Ag NW composite onto stretchable fabric. In addition to enabling the creation of wearable stretchable circuits, Figure 8 shows how patterning

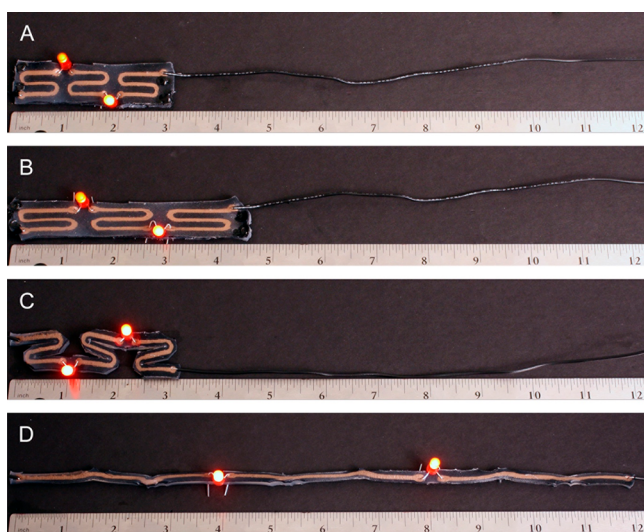


Figure 8. (A) A stretchable LED circuit at 0% and (B) 50% strain. Serpentine variant of stretchable LED circuit at (C) 0% (D) 300% strain.

onto fabric can be used to create conductive traces that enable much greater stretchability than can be achieved with the native material. To create the pattern in Figure 8A, the Cu–Ag NWs were filtered through a gasket with serpentine holes onto stretchable fabric, after which the NWs were annealed, and both the NWs and stretch fabric were infiltrated with PDMS. LEDs

were electrically connected to the conductive composite by simply inserting the leads through the material. The lit LEDs illustrate the conductivity of the material and its potential for use in stretchable electronics (Figure 8A). By itself, the fabric–NW composite exhibited a maximum strain of approximate 50%, which was limited by the stretchability of the fabric (Figure 8B). Cutting lines between the conductive traces (Figure 8C) allowed the circuit to unfold and stretch to a strain of 300% (Figure 8D), while retaining enough conductivity to power the red LEDs. Photographs of the serpentine pattern during the strain process (Figure 9A), shows the modes of

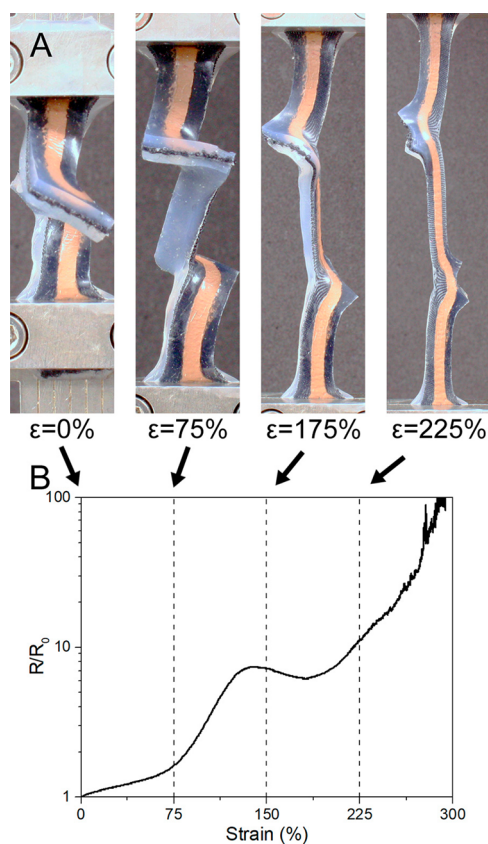


Figure 9. (A) Serpentine Cu–Ag NW trace at various degrees of strain illustrating the unfolding process. (B) Strain vs  $R/R_0$  behavior of the serpentine trace.

twisting, bending, and straining that occurs during the unfolding and stretching of the serpentine pattern. The  $R/R_0$  vs strain behavior (Figure 9B) shows an initial increase to  $\sim 150\%$ , a small decrease in  $R/R_0$  to 175%, and a further increase to 300%. We attribute the flat part of the  $R/R_0$  curve to the untwisting of the serpentine pattern that occurs at 150% strain. These results illustrate not only the extreme stretchability of the patterned composite, but also its ability to retain conductivity during bending and twisting, which are essential modes of motion for wearable electronics.

## CONCLUSIONS

This paper demonstrates that an infiltrated felt of Cu–Ag core–shell nanowires retains its conductivity under strain better than any composite with a conductivity greater than  $1000 \text{ S cm}^{-1}$ , including those using AgMFs at concentrations double that of the Cu–Ag nanowires. Given that the composites reported here exhibit better performance than Ag MFs, and use

15 times less silver, this work demonstrates the potential for Cu–Ag nanowires to serve as a more economical and sustainable filler for stretchable conductors. In addition to high performance, this work shows that increasing the stiffness of the PDMS matrix leads to a greater loss of conductivity under strain. This conductivity loss appears to be due to the formation of voids during stretching, which we attribute to debonding between the PDMS matrix and the nanowires. Finally, we show that the nanowire composite can be patterned to create serpentine circuits that retain their functionality up to strains of 300%. Future work might explore the use of this material in clothing-integrated circuits for wearable electronics.

## MATERIALS AND METHODS

**Cu–Ag NW Synthesis.** Cu–Ag NWs were synthesized *via* a two-step protocol. In a 10 L bottle, 800 mL of 0.1 M copper(II) nitrate hemi(pentahydrate), (Cu(NO<sub>3</sub>)<sub>2</sub>·2H<sub>2</sub>O, Sigma-Aldrich ≥98.0%), 115 mL ethylenediamine (EDA, Sigma, ≥ 99%), and 7.5 L of 8 M sodium hydroxide (NaOH, NOAH Technologies, 99%) solutions were mixed together. Next, 750 mL of 1 g/mL α-D-glucose (Sigma-Aldrich, 96%) solution was added, and the bottle was shaken for 1 min. The bottle was then immediately placed in a 60 °C water bath for 1 h to grow Cu NWs. After the synthesis was complete, the Cu NWs were vacuum filtered using a Buchner funnel and a cloth filter, and rinsed with a solution of 3 wt % 10k MW polyvinylpyrrolidone (PVP, Sigma-Aldrich) and 1 wt % *N,N*-diethylhydroxylamine (DEHA, TCI America, >95.0%) (PVP/DEHA). After filtration, the Cu NW slurry was rinsed off the filter into a 500 mL solution of PVP/DEHA for resuspension. The Cu NWs were then centrifuged at 2000 rpm for 10 min to concentrate and further rinse the NWs, after which they were resuspended in 250 mL of fresh PVP/DEHA solution. This centrifugation process was repeated three times, and the Cu NWs were kept in 250 mL of a PVP/DEHA storage solution. The concentration of the product solution was measured with a PerkinElmer 3100 Atomic Absorption Spectrometer. The observed concentration of the solution was 14.5 mg/mL for a total mass of approximately 3.6 g of Cu NWs.

The Cu NWs were subsequently coated with Ag to form Cu–Ag NWs with a mole ratio of 0.85:0.15 Cu:Ag. The 250 mL solution of Cu NWs in storage solution was diluted with distilled water to 800 mL. This solution was stirred with 1.6 L of 2 wt % PVP in water, and 4.4 L of 1 M ascorbic acid (Duda Energy >99.0%) in water. Then 400 mL of 0.025 M silver nitrate (AgNO<sub>3</sub>, Fisher Scientific, ≥ 99.7%) in water was added dropwise to the stirred solution for 10 min. After the addition of AgNO<sub>3</sub> was complete, the reaction was left to stir for 10 min, and the stirring was turned off to allow the NWs to settle overnight. The reaction vessel was then decanted to remove excess solution, and the remaining NWs were rinsed with DI water and centrifuged at 2000 rpm for 5 min three times to concentrate the NWs into 800 mL of PVP/DEHA storage solution. The average Cu–Ag NW length was 41 ± 14 μm and the average diameter was 239 ± 67 nm.

**Filtration and Infiltration.** Filtration was performed using a Millipore vacuum filter funnel. Nanowires were filtered through a silicone gasket (Fuel Cell Store) onto a 400 × 400 stainless steel wire cloth (McMaster Carr). Test specimen and serpentine holes were cut into the gasket with an Epilog Fusion 60W laser cutter. For filtration, 6 mL of the Cu–Ag NW storage solution was diluted with 40 mL of H<sub>2</sub>O and poured through the filter to make a 250-μm-thick Cu–Ag NW felt. The Cu–Ag NW felt was annealed in an oven at 150 °C for 30 min, and transferred from the cloth to a Teflon sheet in a Petri dish. Samples were infiltrated with a 2:1:1 solution of 2-butanone, PDMS precursor Part A, and PDMS precursor part B. The PDMS precursors Ecoflex 00–30 and Dragon Skin 30 were provided from Smooth-On Inc. The samples were infiltrated for 30 min under ambient conditions, followed by vacuum infiltration for 3 h in a desiccator to allow for solvent evaporation and curing of the PDMS. Scanning electron

microscope images of the felt and the infiltrated composite were taken using an FEI XL30 SEM.

**Electrical and Strain Characterization.** The electrical conductivity of infiltrated and noninfiltrated samples was measured using a four-point probe, and calculated by multiplying the measured sheet resistance by the sample thickness. Stress–strain tests were performed using a microstrain analyzer (MSA, TA Instruments RSA III). Electrical characterization during strain was observed using a Keithley 2401 SourceMeter with LabView 2016 software. In order to establish contact with the sample in the MSA, the handles of the test specimen were coated in colloidal silver paste (Electron Microscopy Sciences), and sandwiched with copper foil to establish electrical contact. Two pieces of silicone gasket were used to electrically isolate the sample from the metal clamps of the MSA. Stress–strain measurements were performed at a rate of 1% strain per second. Cycling tests were performed at a strain rate of 20% per second, and the resistance was recorded while the sample was held at the minimum (0%) and maximum (50% or 100%) strain for five seconds. The position at which the strain was 0% for all cycles was defined as the starting position of the MSA for the initial strain test, even for samples that underwent plastic deformation during cycling. Plastic deformation and time dependent behavior studies were performed at a rate of 20% strain per second; samples were held at a strain of 100% for 5 s.

**Device Manufacturing.** For the LED circuit, a layer of stretchable, 80% nylon, 20% Spandex fabric (Rex Fabrics) was placed between the patterned silicone gasket and the metal cloth. Cu–Ag NWs were filtered onto the fabric, and were annealed after filtration. The fabric and patterned NWs were immersed in Ecoflex in a Teflon well, and vacuum infiltrated for 30 min, followed by 30 min in a 60 °C oven to cure the PDMS. The LEDs were powered using an external power supply with a compliance voltage of 7 V and a compliance current of 15 mA.

## ASSOCIATED CONTENT

### Supporting Information

The Supporting Information is available free of charge on the ACS Publications website at DOI: 10.1021/acsnano.8b00887.

Figures S1–S4 (PDF)

## AUTHOR INFORMATION

### Corresponding Author

\*E-mail: benjamin.wiley@duke.edu.

### ORCID

Matthew J. Catenacci: 0000-0002-6379-478X

Christopher Reyes: 0000-0001-7273-8854

### Notes

The authors declare no competing financial interest.

## ACKNOWLEDGMENTS

This work was supported by an NSF CAREER award (Grant DMR-1253534). M. Catenacci acknowledges support through the SMIF Voucher Program

## REFERENCES

- (1) Sekitani, T.; Nakajima, H.; Maeda, H.; Fukushima, T.; Aida, T.; Hata, K.; Someya, T. Stretchable Active-Matrix Organic Light-Emitting Diode Display Using Printable Elastic Conductors. *Nat. Mater.* **2009**, *8*, 494–499.
- (2) Yamada, T.; Hayamizu, Y.; Yamamoto, Y.; Yomogida, Y.; Izadi-Najafabadi, A.; Futaba, D. N.; Hata, K. A Stretchable Carbon Nanotube Strain Sensor for Human-Motion Detection. *Nat. Nanotechnol.* **2011**, *6*, 296–301.
- (3) Yan, C.; Wang, J.; Kang, W.; Cui, M.; Wang, X.; Foo, C. Y.; Chee, K. J.; Lee, P. S. Highly Stretchable Piezoresistive Graphene–Nanocellulose Nanopaper for Strain Sensors. *Adv. Mater.* **2014**, *26*, 2022–2027.

- (4) Hong, S.; Lee, H.; Lee, J.; Kwon, J.; Han, S.; Suh, Y. D.; Cho, H.; Shin, J.; Yeo, J.; Ko, S. H. Highly Stretchable and Transparent Metal Nanowire Heater for Wearable Electronics Applications. *Adv. Mater.* **2015**, *27*, 4744–4751.
- (5) Joshipura, I. D.; Finn, M.; Tan, S. T. M.; Dickey, M. D.; Lipomi, D. J. Stretchable Bioelectronics—Current and Future. *MRS Bull.* **2017**, *42*, 960–967.
- (6) Xu, S.; Zhang, Y.; Cho, J.; Lee, J.; Huang, X.; Jia, L.; Fan, J. A.; Su, Y.; Su, J.; Zhang, H.; Cheng, H.; Lu, B.; Yu, C.; Chuang, C.; Kim, T.-i.; Song, T.; Shigeta, K.; Kang, S.; Dagdeviren, C.; Petrov, I.; et al. Stretchable Batteries with Self-Similar Serpentine Interconnects and Integrated Wireless Recharging Systems. *Nat. Commun.* **2013**, *4*, 1543–1551.
- (7) Sekitani, T.; Noguchi, Y.; Hata, K.; Fukushima, T.; Aida, T.; Someya, T. A Rubberlike Stretchable Active Matrix Using Elastic Conductors. *Science* **2008**, *321*, 1468–1472.
- (8) Kim, K. H.; Vural, M.; Islam, M. F. Single-Walled Carbon Nanotube Aerogel-Based Elastic Conductors. *Adv. Mater.* **2011**, *23*, 2865–2869.
- (9) Duan, S.; Wang, Z.; Zhang, L.; Liu, J.; Li, C. Three-Dimensional Highly Stretchable Conductors from Elastic Fiber Mat with Conductive Polymer Coating. *ACS Appl. Mater. Interfaces* **2017**, *9*, 30772–30778.
- (10) Stoyanov, H.; Kollosche, M.; Risse, S.; Waché, R.; Kofod, G. Soft Conductive Elastomer Materials for Stretchable Electronics and Voltage Controlled Artificial Muscles. *Adv. Mater.* **2013**, *25*, 578–583.
- (11) Matsuhisa, N.; Kaltenbrunner, M.; Yokota, T.; Jinno, H.; Kuribara, K.; Sekitani, T.; Someya, T. Printable Elastic Conductors with a High Conductivity for Electronic Textile Applications. *Nat. Commun.* **2015**, *6*, 7461–7471.
- (12) Matsuhisa, N.; Inoue, D.; Zalar, P.; Jin, H.; Matsuba, Y.; Itoh, A.; Yokota, T.; Hashizume, D.; Someya, T. Printable Elastic Conductors by In Situ Formation of Silver Nanoparticles from Silver Flakes. *Nat. Mater.* **2017**, *16*, 834–840.
- (13) Oh, Y.; Yoon, I. S.; Lee, C.; Kim, S. H.; Ju, B.-K.; Hong, J.-M. Selective Photonic Sintering of Ag Flakes Embedded in Silicone Elastomers to Fabricate Stretchable Conductors. *J. Mater. Chem. C* **2017**, *5*, 11733–11740.
- (14) Gao, H.-L.; Xu, L.; Long, F.; Pan, Z.; Du, Y.-X.; Lu, Y.; Ge, J.; Yu, S.-H. Macroscopic Free-Standing Hierarchical 3D Architectures Assembled from Silver Nanowires by Ice Templating. *Angew. Chem., Int. Ed.* **2014**, *53*, 4561–4566.
- (15) Ge, J.; Yao, H.-B.; Wang, X.; Ye, Y.-D.; Wang, J.-L.; Wu, Z.-Y.; Liu, J.-W.; Fan, F.-J.; Gao, H.-L.; Zhang, C.-L.; Yu, S.-H. Stretchable Conductors Based on Silver Nanowires: Improved Performance through a Binary Network Design. *Angew. Chem., Int. Ed.* **2013**, *52*, 1654–1659.
- (16) Zhu, C.-H.; Li, L.-M.; Wang, J.-H.; Wu, Y.-P.; Liu, Y. Three-Dimensional Highly Conductive Silver Nanowires Sponges Based on Cotton-Templated Porous Structures for Stretchable Conductors. *RSC Adv.* **2017**, *7*, 51–57.
- (17) Huang, W.; Li, J.; Zhao, S.; Han, F.; Zhang, G.; Sun, R.; Wong, C.-P. Highly Electrically Conductive and Stretchable Copper Nanowires-Based Composite for Flexible and Printable Electronics. *Compos. Sci. Technol.* **2017**, *146*, 169–176.
- (18) Lipomi, D. J.; Vosgueritchian, M.; Tee, B. C. K.; Hellstrom, S. L.; Lee, J. A.; Fox, C. H.; Bao, Z. Skin-Like Pressure and Strain Sensors Based on Transparent Elastic Films of Carbon Nanotubes. *Nat. Nanotechnol.* **2011**, *6*, 788–792.
- (19) Wang, Y.; Zhu, C.; Pfattner, R.; Yan, H.; Jin, L.; Chen, S.; Molina-Lopez, F.; Lissel, F.; Liu, J.; Rabiah, N. I.; Chen, Z.; Chung, J. W.; Linder, C.; Toney, M. F.; Murmann, B.; Bao, Z. A Highly Stretchable, Transparent, and Conductive Polymer. *Sci. Adv.* **2017**, *3*, e1602076.
- (20) Gutowski, T. G.; Sahni, S.; Allwood, J. M.; Ashby, M. F.; Worrell, E. The Energy Required to Produce Materials: Constraints on Energy-Intensity Improvements, Parameters of Demand. *Philos. Trans. R. Soc., A* **2013**, *371*, 20120003.
- (21) Cruz, M. A.; Ye, S.; Kim, M. J.; Reyes, C.; Yang, F.; Flowers, P. F.; Wiley, B. J. Multigram Synthesis of Cu-Ag Core-Shell Nanowires Enables the Production of a Highly Conductive Polymer Filament for 3D Printing Electronics. *Part. Part. Syst. Char.* **2018**, 1700385.
- (22) Stewart, I. E.; Ye, S.; Chen, Z.; Flowers, P. F.; Wiley, B. J. Synthesis of Cu-Ag, Cu-Au, and Cu-Pt Core-Shell Nanowires and Their Use in Transparent Conducting Films. *Chem. Mater.* **2015**, *27*, 7788–7794.
- (23) Savagatrup, S.; Makaram, A. S.; Burke, D. J.; Lipomi, D. J. Mechanical Properties of Conjugated Polymers and Polymer-Fullerene Composites as a Function of Molecular Structure. *Adv. Funct. Mater.* **2014**, *24*, 1169–1181.
- (24) Lee, J.-B.; Khang, D.-Y. Electrical and Mechanical Characterization of Stretchable Multi-Walled Carbon Nanotubes/Polydimethylsiloxane Elastomeric Composite Conductors. *Compos. Sci. Technol.* **2012**, *72*, 1257–1263.
- (25) Lu, N.; Lu, C.; Yang, S.; Rogers, J. Highly Sensitive Skin-Mountable Strain Gauges Based Entirely on Elastomers. *Adv. Funct. Mater.* **2012**, *22*, 4044–4050.
- (26) Zu, M.; Li, Q.; Wang, G.; Byun, J.-H.; Chou, T.-W. Carbon Nanotube Fiber Based Stretchable Conductor. *Adv. Funct. Mater.* **2013**, *23*, 789–793.
- (27) Chen, M.; Zhang, L.; Duan, S.; Jing, S.; Jiang, H.; Luo, M.; Li, C. Highly Conductive and Flexible Polymer Composites with Improved Mechanical and Electromagnetic Interference Shielding Performances. *Nanoscale* **2014**, *6*, 3796–3803.
- (28) Zhao, S.; Li, J.; Cao, D.; Zhang, G.; Li, J.; Li, K.; Yang, Y.; Wang, W.; Jin, Y.; Sun, R.; Wong, C.-P. Recent Advancements in Flexible and Stretchable Electrodes for Electromechanical Sensors: Strategies, Materials, and Features. *ACS Appl. Mater. Interfaces* **2017**, *9*, 12147–12164.
- (29) Rosset, S.; Niklaus, M.; Dubois, P.; Shea, H. R. Metal Ion Implantation for the Fabrication of Stretchable Electrodes on Elastomers. *Adv. Funct. Mater.* **2009**, *19*, 470–478.
- (30) Gent, A. N.; Park, B. Failure Processes in Elastomers at or Near a Rigid Spherical Inclusion. *J. Mater. Sci.* **1984**, *19*, 1947–1956.
- (31) Ahagon, A.; Gent, A. N. Effect of Interfacial Bonding on the Strength of Adhesion. *J. Polym. Sci., Polym. Phys. Ed.* **1975**, *13*, 1285–1300.
- (32) Lessing, J.; Morin, S. A.; Keplinger, C.; Tayi, A. S.; Whitesides, G. M. Stretchable Conductive Composites Based on Metal Wools for Use as Electrical Vias in Soft Devices. *Adv. Funct. Mater.* **2015**, *25*, 1418–1425.
- (33) Hansen, T. S.; West, K.; Hassager, O.; Larsen, N. B. Highly Stretchable and Conductive Polymer Material Made from Poly(3,4-ethylenedioxythiophene) and Polyurethane Elastomers. *Adv. Funct. Mater.* **2007**, *17*, 3069–3073.
- (34) Araki, T.; Sugahara, T.; Nogi, M.; Suganuma, K. Effect of Void Volume and Silver Loading on Strain Response of Electrical Resistance in Silver Flakes/Polyurethane Composite for Stretchable Conductors. *Jpn. J. Appl. Phys.* **2012**, *51*, 11PD01.
- (35) Yamaguchi, K.; Busfield, J. J. C.; Thomas, A. G. Electrical and Mechanical Behavior of Filled Elastomers. I. The Effect of Strain. *J. Polym. Sci., Part B: Polym. Phys.* **2003**, *41*, 2079–2089.
- (36) Hanson, D. E.; Hawley, M.; Houlton, R.; Chitanvis, K.; Rae, P.; Orler, E. B.; Wroblecki, D. A. Stress Softening Experiments in Silica-Filled Polydimethylsiloxane Provide Insight into a Mechanism for the Mullins Effect. *Polymer* **2005**, *46*, 10989–10995.
- (37) Cantournet, S.; Desmorat, R.; Besson, J. Mullins Effect and Cyclic Stress Softening of Filled Elastomers by Internal Sliding and Fictitious Thermodynamics Model. *Int. J. Solids Struct.* **2009**, *46*, 2255–2264.
- (38) Fukahori, Y. New Progress in the Theory and Model of Carbon Black Reinforcement of Elastomers. *J. Appl. Polym. Sci.* **2005**, *95*, 60–67.
- (39) Liu, C.-X.; Choi, J.-W. Analyzing Resistance Response of Embedded PDMS and Carbon Nanotubes Composite Under Tensile Strain. *Microelectron. Eng.* **2014**, *117*, 1–7.

(40) Wang, C.; Li, X.; Gao, E.; Jian, M.; Xia, K.; Wang, Q.; Xu, Z.; Ren, T.; Zhang, Y. Carbonized Silk Fabric for Ultrastretchable, Highly Sensitive, and Wearable Strain Sensors. *Adv. Mater.* **2016**, *28*, 6640–6648.

(41) Zhang, M.; Wang, C.; Wang, Q.; Jian, M.; Zhang, Y. Sheath–Core Graphite/Silk Fiber Made by Dry-Meyer-Rod-Coating for Wearable Strain Sensors. *ACS Appl. Mater. Interfaces* **2016**, *8*, 20894–20899.